NJC

PAPER

View Article Online
View Journal | View Issue

Cite this: *New J. Chem.*, 2019, **43**, 8551

Combined photoanodes of TiO_2 nanoparticles and {001}-faceted TiO_2 nanosheets for quantum dot-sensitized solar cells

Qiqian Gao,[a] Xiaojuan Sun,[b] Xijia Yang,*[a] Liying Wang,[a] Xuesong Li,[a] Xueyu Zhang,[a] Lianfeng Duan[a] and Wei Lü*[a]

Received 30th March 2019,
Accepted 30th April 2019

DOI: 10.1039/c9nj01644a

rsc.li/njc

A key point for constructing quantum dot-sensitized solar cells (QDSSCs) with high efficiency is to improve the utilization of sunlight. While various TiO_2 morphologies such as nanoparticles, nanosheets, nanotubes and nanorods have been used as photoanodes of QDSSCs for improving cell performance, these investigations are generally focused on a single morphology of TiO_2. Herein, a combined photoanode structure based on TiO_2 nanoparticles and {001}-faceted TiO_2 nanosheets have been designed, which exhibits improvement in cell performance. Owing to the strong light scattering and fast electron transfer ability of TiO_2 nanosheets, an optimal power conversion efficiency of 4.98% with a short circuit current density (J_{sc}) of 17.57 mA cm^{-2}, an open circuit voltage (V_{oc}) of 0.63 V and a fill factor (FF) of 0.45 is achieved compared to the TiO_2 nanoparticle photoanode (3.61%). The present work offers a feasible method towards improving the efficiency of QDSSCs.

1. Introduction

Quantum dot-sensitized solar cells (QDSSCs) have attracted great attention as a candidate of novel photovoltaic devices. The advantages of semiconductor quantum dots (QDs) such as tunable band gap, high molar extinction coefficients and multiple exciton generation[1–4] allow QDSSCs to achieve a theoretical power conversion efficiency (PCE) of 44%, which is higher than that of single p–n junction photovoltaic devices (33%).[5,6] Despite the above mentioned advantages, the highest power conversion efficiency (PCE) of QDSSCs is still lower than those of perovskite solar cells (PSCs) and dye-sensitized solar cells (DSSCs).[7–10] This is mainly due to optical loss, unsophisticated cell configuration, and serious charge recombination.[11–14]

To boost the PCE of QDSSCs, great efforts have been dedicated to the optimization of photoanode structure. The physical structure of QDSSCs is a sandwich construction consisting of a counter electrode (CE), a photoanode and an electrolyte which is similar to that of DSSCs. TiO_2, acting as the photoanode matrix, is the most successful photoanode material to date, and it is involved in extracting, collecting and transferring light-generated electrons to the external circuit. In order to obtain higher PCE, different morphologies of TiO_2 have been prepared and applied as the photoanodes of QDSSCs such as nanoparticles, nanosheets, nanotubes and nanorods and so on.[15–26] Generally, these investigations are focused on a single morphology of TiO_2. Recently, several groups reported the combined structures of TiO_2 with different morphologies as photoanodes of DSSCs to further improve the photoelectrical performance. Min Zhu *et al.* designed and prepared a nanorod/nanoparticle double-deck composite architecture and obtained a PCE of 3.25% in DSSCs.[27] Hyung-Kook Kim *et al.* reported a photoelectrode based on a TiO_2 nanofiber/nanoparticle composite. The PCE was increased to 38.6% due to the strong scattering effect of the nanofibers.[28] Yoon-Bong Hahn *et al.* investigated a TiO_2 nanoparticle/nanotube/Ag composite photoanode and obtained an improved J_{sc} of 16.46 mA cm^{-2} in DSSCs.[29] Haijun Su *et al.* confirmed the rapid electron transport in TiO_2 nanowire/nanoparticle composites in DSSCs and achieved a PCE of 5.84%.[30] The above mentioned studies are mainly focused on DSSCs. For QDSSCs, few reports on combined photoanodes of TiO_2 with different morphologies could be found. Very recently, TiO_2 nanowire/nanotube photoanodes, hierarchical TiO_2 nanoflower/nanorod photoanodes, TiO_2 3D hierarchical branched nanowire/hollow sphere photoanodes, and TiO_2 hierarchical pore/nanorod photoanodes were used in QDSSCs.[31–36] However, the utilization of nanofibers, nanorods, nanotubes and nanowires could decrease the specific surface area of the TiO_2 film to a large extent. Therefore, further investigation of combined photoanodes with TiO_2 with different morphologies is still important for further improvement of QDSSC performance.

[a] *Key Laboratory of Advanced Structural Materials, Ministry of Education & Advanced Institute of Materials Science, Changchun University of Technology, Changchun 130012, China. E-mail: yangxijia@ccut.edu.cn, lw771119@hotmail.com; Fax: +86-0431-85716426; Tel: +86-0431-85716421*

[b] *State Key Laboratory of Luminescence and Applications, Changchun Institute of Optics, Fine Mechanics and Physics, Chinese Academy of Sciences, Changchun 130012, China*

Herein, we design a mesoporous film consisting of TiO_2 nanoparticles (NPs) and {001}-faceted TiO_2 nanosheets (NSs). TiO_2 NPs could provide active sites for depositing QDs, and TiO_2 NSs are responsible for offering a direct transmission channel for excited electrons. In addition, NSs are helpful for sunlight reutilization due to their outstanding light scattering ability. With CuS as a counterelectrode and a polysulfide solution as an electrolyte, a champion PCE up to 4.98% (V_{oc} = 0.63 V, J_{sc} = 17.57 mA cm^{-2}) is achieved, and a 37.9% improvement in cell efficiency is obtained. The novel structure offers a feasible method for improving the efficiency of QDSSCs.

2. Experimental

2.1. Materials

Isopropyl alcohol, tetrabutyl titanate and glacial acetic acid were bought from Tianjin Fuyu Fine Chemical. Sodium thiosulfate pentahydrate, cupric sulfate and Se powder were purchased from Tianjin Guangfu Fine Chemical Research Institute. Absolute ethyl alcohol, hydrofluoric acid, methyl alcohol and acetone were provided by Beijing Chemical Works. Sodium sulfide nanohydrate and zinc acetate dihydrate were offered by Xilong Scientific. Cadmium acetate dihydrate, sodium sulfite, titanium oxide (25 nm, anatase), ethyl cellulose and terpinoel were provided by Aladdin Industrial Corporation. Sulfur sublimed was bought from Tianjin Fuchen Chemical Reagents Factory. Trisodium nitrilotriacetate monohydrate was offered by TCI Shanghai. FTO conducting glass (<15 Ohm sq^{-1}, 1.6 mm in thickness) was provided by Zhuhai Kaivo. Deionized water was prepared using a laboratory water purification system (HTECH).

2.2. Synthesis of TiO_2 NSs

TiO_2 NSs were prepared by hydrothermal synthesis. In detail, 4 ml tetrabutyl titanate ($C_{16}H_{36}O_4Ti$) was dissolved in 15 ml isopropyl alcohol (C_3H_8O) under stirring for half an hour. Then, 0.5 ml hydrofluoric acid (HF) was added. The obtained solution was transferred into a 50 ml sealed Teflon reactor and sintered at 180 °C for 12 h. The obtained white powders were washed and dried at 60 °C for 12 hours.

2.3. Preparation of a TiO_2 film consisting of NPs and NSs

TiO_2 paste was prepared by mixing 1.67 g terpinoel, 0.2 g ethyl cellulose, 0.4 g TiO_2 and 2 ml absolute ethyl alcohol under stirring for 24 h. A mesoporous TiO_2 film was prepared by spin-coating followed by sintering for 1 h at 500 °C. For TiO_2 films consisting of NPs and NSs, different mass ratios of NP to NS were used to prepare TiO_2 paste. Samples with mass ratios of NP to NS of 5 : 0, 4 : 1, 3 : 2, 2 : 3, 1 : 4 and 0 : 5 were defined as S1, S2, S3, S4, S5 and S6 respectively.

2.4. Assembly of QDSSCs

CdSe/CdS/ZnS QDs, CuS counter electrodes (CEs), and electrolyte were prepared using the method reported in our previous work.[37] The photoanode, CEs and electrolyte were fabricated into a sandwiched cell structure with a polymer spacer in between. The detailed assembly process is shown in Scheme 1.

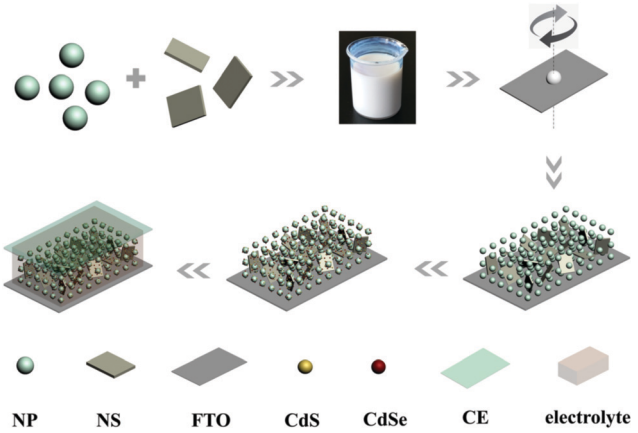

Scheme 1 Preparation processes of QDSSCs.

2.5. Characterization

The morphology and structure of samples were characterized by transmission electron microscopy (TEM) (Tecnai F20), field emission scanning electron microscopy (FESEM, S4800, Hitachi) and X-ray diffraction (D-MAX II A X-ray diffractometer). The specific surface area and pore diameter distribution of the mesoporous TiO_2 membrane were analyzed using TriStar II 3020. The light absorption and diffuse reflection properties of the photoanodes were tested using a UV/Vis-NIR spectrophotometer (UV-3150). The cell performances were measured using a solar cell scan 100, solar cell QE/IPCE measurement system (Zolix Instruments Co.,Ltd), a Zolix ss150 solar simulator and an electrochemical workstation (CHI660E).

3. Results and discussion

Fig. 1 shows the top-view SEM images of S1, S4, and S6 and the corresponding cross-section images. For the pure NP film S1 shown in Fig. 1(a), a typical mesoporous structure could be

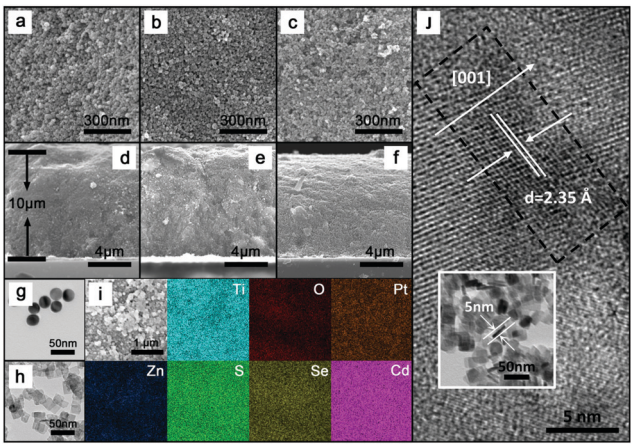

Fig. 1 SEM images showing the top and cross section view of S1 (a and d), S4 (b and e) and S6 (c and f). TEM images of NPs (g) and NSs (h). (i) EDX mapping images of S4 after QD deposition. HRTEM image of NSs (j), inset is the TEM image of NSs.

observed. With the increasing loading amount of NSs in the photoanode, a comparatively even surface could be observed along with some large holes as shown in Fig. 1(b and c), which is attributed to the addition of NSs, and induces a variation of the specific surface area as shown later. From the cross-sectional view, it can be observed that the thickness of the TiO_2 film is ~10 μm. Fig. 1(g and h) show the TEM images of TiO_2 NPs and NSs. Sphere and sheet morphologies could be confirmed, indicating the successful synthesis of NSs. In order to confirm the successful deposition of QDs, EDX mapping images of S4 are shown in Fig. 1(i). The distribution of Ti, O, Zn, S, Se and Cd elements in mesoporous TiO_2 could be confirmed. The HRTEM image of NSs shown in Fig. 1(j) directly shows that the lattice spacing with a distance of 2.35 Å corresponding to the (001) planes of anatase TiO_2 is parallel to the bottom and top facets, which indicates that the NSs are {001}-faceted, respectively.[38–40] The inset in Fig. 1(j) shows a typical TEM image of a NS at a standing angle indicating that the thickness of the NS is about 5 nm.

The XRD patterns of S1, S2, S3, S4, S5, S6 and FTO are shown in Fig. 2(a). For bare FTO, peaks located at 65.58°, 61.71°, 51.51°, 37.87° and 26.54° correspond to the (301), (310), (221), (200) and (110) crystal planes of rutile SnO_2 (JCPDS no. 41-1445).[41] After coating with a mesoporous TiO_2 film, additional diffraction peaks could be observed and could be indexed to the anatase structure (JCPDS card 21-1272), indicating that the as-prepared NSs are an anatase crystalline structure.[42] With the increasing mass of NSs in the photoanode, the peak related to the (101) crystal plane diffraction becomes evident, demonstrating prior growth along the [100] direction of NSs.[43]

Fig. 2(b and c) show the specific surface area and porosity curves of S1 and S6. It could be observed from Fig. 2(b) that S1 has a specific surface area of 87.7166 $m^2 g^{-1}$, and that of S6 is 64.6781 $m^2 g^{-1}$. Due to the sheet morphology of NSs, the addition of NSs would induce a stacked structure between the NSs, thus decreasing the specific surface area of the film. Inversely, the pore diameters increase with increasing NS amount in photoanodes. S1 has a pore diameter of 22.38 nm and that of S6 is 30.33 nm, which is consistent with SEM results. The larger pore size would be beneficial for wetting between the photoanode and the electrolyte. However, the small specific surface area induced by NS addition would decrease the active sites for QD deposition. Therefore, the optimal NS amount in the photoanodes should be decided by a performance test.

The optical properties of different samples are investigated by UV-visible absorption spectroscopy and the spectra are shown in Fig. 3(a and b). Upon increasing the mass ratio of NSs to sample S4, the UV-vis absorption spectra show a redshift and increased absorption. Further increasing the NS amount results in a decrease in the absorption. After the deposition of QDs as shown in Fig. 3(b), the absorption range is expanded to about 650 nm due to the visible light absorption ability of QDs. Also, upon increasing the mass ratio of NS to sample S4,

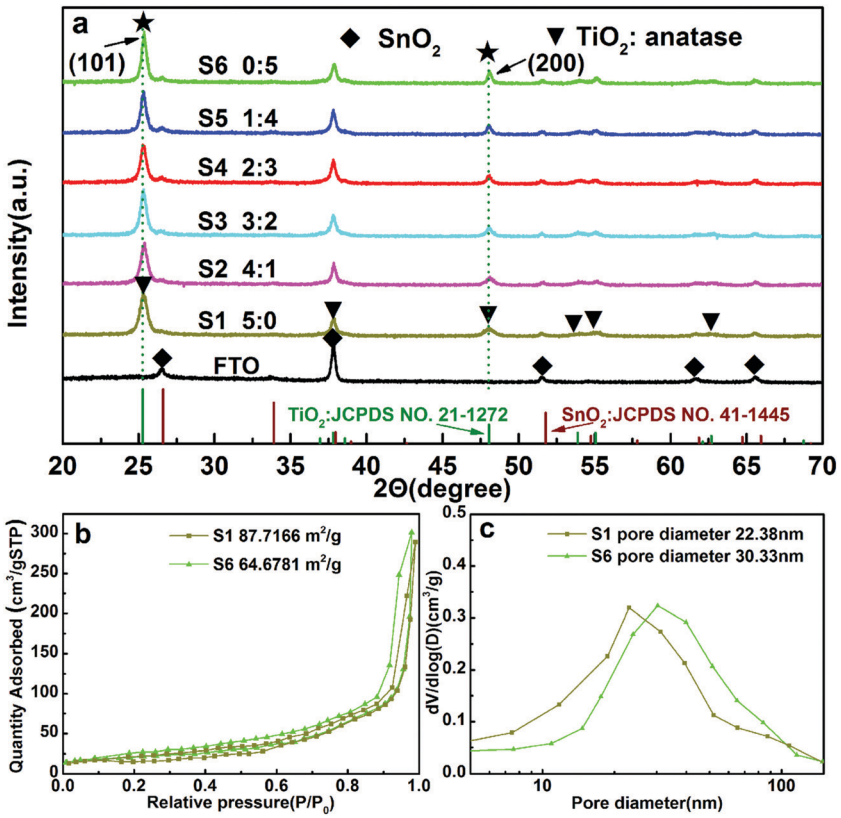

Fig. 2 XRD patterns (a) of samples with different NS amounts in photoanodes; N_2 adsorption–desorption isotherm (b) and pore size distribution (c) curves of S1 and S6.

the UV-vis absorption spectra show a redshift and increased absorption. Sample S4 shows the highest light absorption. The improved absorbance can be attributed to two reasons: (i) a larger pore diameter which, as observed in Fig. 1(b) and 2(c), can improve the permeation between the TiO_2 film and the QD precursor solution, which is beneficial for the deposition of QDs. (ii) The outstanding light scattering effect of NSs can realize secondary utilization of sunlight and reduce light loss.[44] Further increasing the NS amount results in a decrease in the absorption. As mentioned previously, the significantly reduced specific surface area induced by NS addition would decrease the active sites for QD deposition, which could be the reason for the decrease in absorption.

TiO_2 NSs have been proved to increase the scattering ability of the film compared with TiO_2 NPs.[45,46] In the present work, the prepared mesoporous TiO_2 film consisting of NPs and NSs is also expected to show better light scattering properties. Herein, the diffuse reflectance spectra of six samples before and after QD deposition are measured using a UV/Vis-NIR spectrophotometer and shown in Fig. 3(c and d). The higher diffuse reflection is beneficial to improve the optical path to achieve secondary utilization of sunlight. Without QD deposition, the diffuse reflection monotonously increases with the increasing mass ratio of NSs in photoanodes as shown in Fig. 3(c), which is consistent with a previous report. After QD deposition, inverse phenomena are observed. The diffuse reflection monotonously decreases with the increasing mass ratio of NSs in photoanodes as shown in Fig. 3(d), which could result due to the small specific surface area of the film, thus inducing insufficient QD deposition.

Fig. 4(a and b) show the results of *J–V* and incident photon-to-current conversion efficiency (IPCE). The detailed photovoltaic parameters are shown in Table 1. The J_{sc} shows an increasing tendency followed by a decrease with the increasing mass ratio of NSs in photoanodes. The increase in J_{sc} is due to the excellent electron transmission ability and light scattering performance of NSs. The electrons transferred in NSs which possess a direct channel can avoid the grain boundary which is plentiful in NPs.

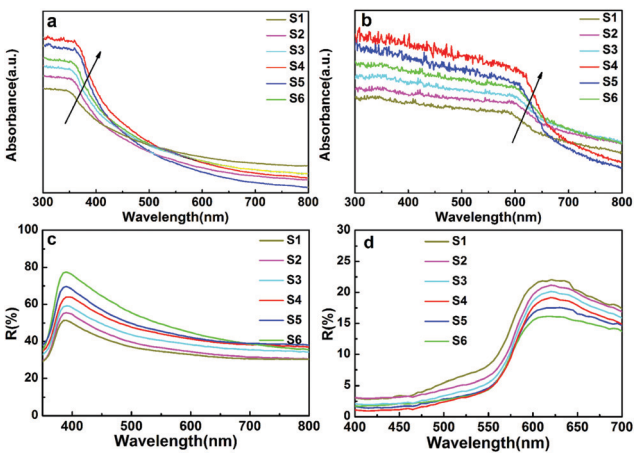

Fig. 3 UV-visible absorption spectra of S1, S2, S3, S4, S5, S6 before (a) and after (b) QD deposition; diffuse reflectance spectra of S1, S2, S3, S4, S5, S6 before (c) and after (d) QD deposition.

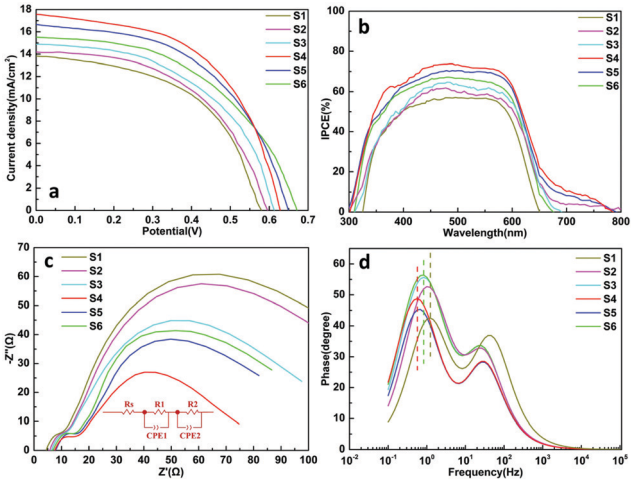

Fig. 4 *J–V* (a) and IPCE (b) curves of cells fabricated based on S1, S2, S3, S4, S5 and S6; Nyquist plots (c) and Bode phase plots (d) of cells fabricated based on S1, S2, S3, S4, S5 and S6, the illustration is the equivalent circuit diagram.

Table 1 *J–V* parameters of cells fabricated based on S1, S2, S3, S4, S5 and S6

Sample	Mass ratio of NPs to NSs	PCE (%)	J_{sc} (mA cm^{-2})	FF	V_{oc} (V)
S1	5 : 0	3.61	13.82	0.45	0.58
S2	4 : 1	3.80	14.32	0.45	0.59
S3	3 : 2	4.08	14.88	0.45	0.61
S4	2 : 3	4.98	17.57	0.45	0.63
S5	1 : 4	4.72	16.49	0.44	0.65
S6	0 : 5	4.57	15.50	0.44	0.67

The addition of excess NSs results in a small specific surface area of the film inducing insufficient QD deposition, thus decreasing the carrier concentration in the photoanode. The IPCE curves in Fig. 4(b) are consistent with the tendency of J_{sc}. A continuous increase in V_{oc} up to 0.67 V is observed. This indicates that 2D TiO_2 which possesses a larger pore size can contribute to the V_{oc}. These results indicate that the mixing of NPs and NSs is favorable for PCE.

To further investigate the effect of the mesoporous TiO_2 film on the photoelectric properties of QDSSCs, electrochemical impedance spectroscopy (EIS) is performed and Nyquist plots and Bode phase plots are determined to reveal the electron transport process. Detailed impedance parameters are listed in Table 2. As shown in Fig. 4(c), the larger semicircle in the low frequency region corresponds to charge transfer resistance (R_2) at the TiO_2/QDs/electrolyte interface.[47,48] It is worth noticing that S4 shows a minimum value of 57.1 Ω, indicating that NSs

Table 2 Impedance parameters of cells fabricated based on S1, S2, S3, S4, S5 and S6

Sample	Mass ratio of NPs to NSs	R_1 (Ω)	R_2 (Ω)	τ_e (ms)
S1	5 : 0	7.805	122.3	131.3
S2	4 : 1	7.711	114.8	159.2
S3	3 : 2	7.391	89.8	176.8
S4	2 : 3	7.058	57.1	283.2
S5	1 : 4	7.352	76.6	233.6
S6	0 : 5	7.243	95.3	192.8

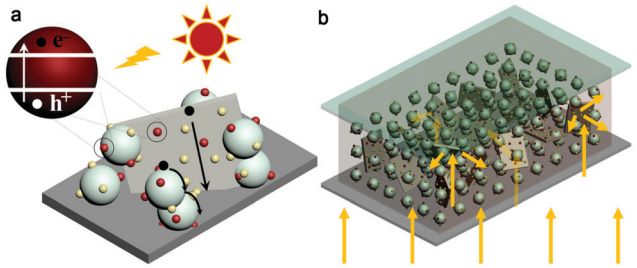

Fig. 5 Schematic illustration of the electron transfer path (a) and light scattering properties (b).

benefit the reduction of charge transfer resistance. The smaller semicircle is related to the charge-transfer resistance at the CE/electrolyte interface. Only a slight difference could be observed between them because we used the same polysulfide electrolyte and CuS counter electrode.

The Bode plot shown in Fig. 4(d) provides the electron lifetime (τ_e) in QDSSCs according to the following equation: $\tau_e = 1/(2\pi f_{max})$, where f_{max} represents the characteristic frequency at the peak of the middle-frequency range.[49] The τ_e values of QDSSCs made from S1, S2, S3, S4, S5 and S6 electrodes are calculated to be 131.3, 159.2, 176.8, 283.2, 233.6, and 192.8 ms respectively. S4 shows the longest τ_e indicating a lower recombination rate of electrons, which is consistent with the analysis of R_2. The longer τ_e can be attributed to direct electron transmission channels offered by NSs.

Fig. 5(a and b) show the electron transfer path and light scattering mechanism of photoanodes. There is an obvious difference in the electron transport route for two kinds of TiO_2 morphologies. TiO_2 NSs can serve as a direct channel for photogenerated electrons, whereas in TiO_2 NPs, injected electrons need to pass through plentiful grain boundaries which can lead to serious charge recombination and loss, thus reducing the electron lifetime significantly and further decreasing J_{sc}. The advantages of TiO_2 NSs are: (1) TiO_2 NSs could increase the scattering ability of the film compared with TiO_2 NPs. High diffusion reflection is beneficial to improve the optical path to achieve secondary utilization of sunlight. (2) TiO_2 NSs serve as a direct channel for the photogenerated electrons thus avoiding the photoelectron loss during transport. The shortcoming of TiO_2 NSs is that the stacking between sheets would decrease the specific surface area of the film thus hindering QD deposition, which induces a low carrier concentration in photoanodes. Therefore, an appropriate ratio of NPs to NSs should be adopted to achieve the best cell performance as discussed in the present work. As shown in Fig. 5(b), NSs possess a longer light path and ensure the capture of sunlight into the photoanode. Better light scattering properties of the mesoporous TiO_2 film consisting of NPs and NSs could improve the J_{sc} of QDSSCs effectively.

4. Conclusions

In summary, TiO_2 NSs were synthesised and combined with TiO_2 NPs to prepare a mesoporous TiO_2 film. A 37.9% enhancement in power conversion efficiency was observed compared to that of a pure TiO_2 NP photoanode. The improved cell performance is due to the outstanding light scattering effect and excellent electronic transmission capability of TiO_2 NSs. In addition, addition of NSs induces a larger pore diameter of the film, which is favorable for the contact of the electrolyte and the photoanode. This work describes a feasible method towards improving the efficiency of QDSSCs and efficient utilization of solar energy.

Conflicts of interest

There are no conflicts to declare.

Acknowledgements

This work was supported by the National Nature Science Foundation of China (Grant No. 61604017, No. 61574021, No. 61774022), open subject of State Key Laboratory of Luminescence and Applications, Changchun Institute of Optics, Fine Mechanics and Physics, Chinese Academy of Sciences, and the State Scholarship Fund of China Scholarship Council (Grant No. 201408220025).

References

1 Y. B. Lu, L. Li, S. C. Su, Y. J. Chen, Y. L. Song and S. J. Jiao, *RSC Adv.*, 2017, **7**, 9795–9802.
2 K. Veerathangam, M. S. Pandian and P. Ramasamy, *J. Alloys Compd.*, 2018, **735**, 202–208.
3 H. J. Kim, G. C. Xu, C. V. V. M. Gopi, H. Seo, M. Venkata-Haritha and M. Shiratani, *J. Electroanal. Chem.*, 2017, **788**, 131–136.
4 B. L. Yuan, Q. Q. Gao, X. Y. Zhang, L. F. Duan, L. Chen, Z. Mao, X. S. Li and W. Lü, *Electrochim. Acta*, 2018, **277**, 50–58.
5 M. C. Beard, *J. Phys. Chem. Lett.*, 2011, **2**, 1282–1288.
6 W. Shockley and H. J. Queisser, *J. Appl. Phys.*, 1961, **32**, 510–519.
7 S. Jiao, J. Du, Z. L. Du, D. H. Long, W. Y. Jiang, Z. X. Pan, Y. Li and X. H. Zhong, *J. Phys. Chem. Lett.*, 2017, **8**, 559–564.
8 Z. X. Pan, H. S. Rao, I. Mora-Seró, J. Bisquert and X. H. Zhong, *Chem. Soc. Rev.*, 2018, **47**, 7659–7702.
9 W. S. Yang, J. H. Noh, N. J. Jeon, Y. C. Kim, S. Ryu, J. Seo and S. Seok, *Science*, 2015, **348**, 1234–1237.
10 K. Kakiage, Y. Aoyama, T. Yano, K. Oya, J. Fujisawa and M. Hanaya, *Chem. Commun.*, 2015, **51**, 15894–15897.
11 I. Sisman, O. Tekir and H. Karaca, *J. Power Sources*, 2017, **340**, 192–200.
12 K. F. Wang, J. Q. Jiang, S. J. Wan and J. Zhai, *Electrochim. Acta*, 2015, **155**, 357–363.
13 S. Sajid, A. M. Elseman, H. Huang, J. Ji, S. Y. Dou, H. R. Jiang, X. Liu, D. Wei, P. Cui and M. C. Li, *Nano Energy*, 2018, **51**, 408–424.
14 Q. Q. Gao, X. Y. Zhang, L. F. Duan, X. J. Li, X. S. Li, Y. Yang, Q. Yu and W. Lü, *J. Alloys Compd.*, 2017, **715**, 337–343.

15 N. Singh, Z. Salam, A. Subasri, N. Sivasankar and A. Subramania, *Sol. Energy Mater. Sol. Cells*, 2018, **179**, 417–426.
16 T. You, L. Jiang, K. L. Han and W. Q. Deng, *Nanotechnology*, 2013, **24**, 245401.
17 L. F. Duan, L. J. Zhao, H. Cong, X. Y. Zhang, W. Lü and C. L. Xue, *Small*, 2019, 1804347.
18 X. Y. Zhang, S. H. Sun, X. J. Sun, Y. R. Zhao, L. Chen, Y. Yang, W. Lü and D. B. Li, *Light: Sci. Appl.*, 2016, **5**, e16130.
19 Y. L. Sun, X. T. An, L. Chen, Q. Q. Gao, X. Y. Zhang, L. F. Duan and W. Lü, *Mater. Res. Lett.*, 2018, **6**, 314–320.
20 D. R. Baker and P. V. Kamat, *Adv. Funct. Mater.*, 2009, **19**, 805–811.
21 D. P. Wu, X. L. Wang, Y. P. An, X. H. Song, N. Liu, H. J. Wang, Z. Y. Gao, F. Xu and K. Jiang, *Electrochim. Acta*, 2017, **248**, 79–89.
22 D. P. Wu, J. J. He, S. Zhang, K. Cao, Z. Y. Gao, F. Xu and K. Jiang, *J. Power Sources*, 2015, **282**, 202–210.
23 D. P. Wu, Y. X. Wang, N. N. Ma, K. Cao, W. C. Zhang, J. L. Chen, D. Q. Wang, Z. Y. Gao, F. Xu and K. Jiang, *Electrochim. Acta*, 2019, DOI: 10.1016/j.electacta.2019.03.077.
24 D. P. Wu, X. J. Shi, H. Dong, F. Zhu, K. Jiang, D. S. Xu, X. C. Ai and J. P. Zhang, *J. Mater. Chem. A*, 2014, **2**, 16276–16284.
25 D. P. Wu, X. L. Wang, K. Cao, Y. P. An, X. H. Song, N. Liu, F. Xu, Z. Y. Gao and K. Jiang, *Electrochim. Acta*, 2017, **231**, 1–12.
26 D. P. Wu, K. Cao, F. J. Wang, H. J. Wang, Z. Y. Gao, F. Xu, Y. M. Guo and K. Jiang, *Chem. Eng. J.*, 2015, **280**, 441–447.
27 M. Zhu, L. Chen, H. B. Gong, M. Zi and B. Q. Cao, *Ceram. Int.*, 2014, **40**, 2337–2342.
28 H. H. T. Vu, T. S. Atabaev, D. Pham-Cong, M. A. Hossain, D. Y. Lee, N. N. Dinh, C. R. Cho, H. K. Kim and Y. H. Hwang, *Electrochim. Acta*, 2016, **193**, 166–171.
29 W. Y. Rho, H. S. Kim, W. J. Chung, J. S. Suh, B. H. Jun and Y. B. Hahn, *Appl. Surf. Sci.*, 2018, **429**, 23–28.
30 M. Guo, L. Yang, J. Chen, J. Zhang, H. J. Su, L. Liu and K. Y. Xie, *J. Nanosci. Nanotechnol.*, 2018, **18**, 8337–8344.
31 Z. Li, L. B. Yu, Y. B. Liu and S. Q. Sun, *Electrochim. Acta*, 2014, **129**, 379–388.
32 L. B. Yu, Z. Li, Y. B. Liu, F. Cheng and S. Q. Sun, *Appl. Surf. Sci.*, 2014, **305**, 359–365.
33 D. P. Wu, S. Zhang, S. W. Jiang, J. J. He and K. Jiang, *J. Alloys Compd.*, 2015, **624**, 94–99.
34 Y. Xu, W. Wu, H. Rao, H. Chen, D. Kuang and C. Su, *Nano Energy*, 2015, **11**, 621–630.
35 X. L. Zhang, Y. Lin, J. H. Wu, J. Jing and B. P. Fang, *Opt. Commun.*, 2017, **395**, 117–121.
36 X. Du, L. Zhao, X. He, H. Chen, W. X. Li and W. Fang, *J. Energy Chem.*, 2018, **9**, 56–62.
37 Q. Q. Gao, L. F. Duan, X. Y. Zhang, I. Kamiya and W. Lü, *Superlattices Microstruct.*, 2017, **109**, 860–868.
38 L. Wang, D. P. Wu, Z. Guo, J. J. Yan, Y. S. Hu, Z. Chang, Q. P. Yuan, H. Ming and J. S. Wang, *J. Alloys Compd.*, 2018, **745**, 26–32.
39 D. P. Wu, X. L. Wang, Y. P. An, X. H. Song, N. Liu, H. J. Wang, Z. Y. Gao, F. Xu and K. Jiang, *Electrochim. Acta*, 2017, **248**, 79–89.
40 J. G. Yu, J. J. Fan and K. L. Lv, *Nanoscale*, 2010, **2**, 2144–2149.
41 L. B. Yu, Z. Li, Y. B. Liu, F. Cheng and S. Q. Sun, *Appl. Surf. Sci.*, 2014, **309**, 255–262.
42 Y. G. Rong, Z. L. Ku, A. Y. Mei, T. F. Liu, M. Xu, S. Ko, X. Li and H. W. Han, *J. Phys. Chem. Lett.*, 2014, **5**, 2160–2164.
43 B. X. Lei, X. F. Zheng, H. K. Qiao, Y. Li, S. N. Wang, G. L. Huang and Z. F. Sun, *Electrochim. Acta*, 2014, **149**, 264–270.
44 Q. Q. Gao, L. Y. Wang, X. Y. Zhang, L. F. Duan, X. S. Li, X. J. Yang and W. Lü, *New J. Chem.*, 2019, **43**, 5374–5381.
45 Y. H. Zhang, J. G. Cai, Y. R. Ma and L. M. Qi, *Nano Res.*, 2017, **10**, 2610–2625.
46 W. Q. Wu, Y. F. Xu, H. S. Rao, C. Y. Su and D. B. Kuang, *Nanoscale*, 2013, **5**, 4362–4369.
47 B. T. Liu and J. Y. Liou, *Electrochim. Acta*, 2018, **261**, 421–427.
48 M. A. K. L. Dissanayake, J. M. K. W. Kumari, G. K. R. Senadeera and C. A. Thotawatthage, *J. Appl. Electrochem.*, 2016, **46**, 47–58.
49 W. G. Wang, H. Y. Zhang, R. Wang, M. Feng and Y. M. Chen, *Nanoscale*, 2014, **6**, 2390–2396.

